Published in final edited form as:

J Phys Chem B. 2015 October 29; 119(43): 13742–13754. doi:10.1021/acs.jpcb.5b03559.

Removal of Ca^{2+} from the Oxygen-Evolving Complex in Photosystem II Has Minimal Effect on the Mn_4O_5 Core Structure: A Polarized Mn X-ray Absorption Spectroscopy Study

Thomas Lohmiller[†], **Megan L. Shelby**[‡], **Xi Long**[§], **Vittal K. Yachandra**[*], and **Junko Yano**[*]

Physical Biosciences Division, Lawrence Berkeley National Laboratory, Berkeley, California 94720-5230, United States

Abstract

Ca^{2+}-depleted and Ca^{2+}-reconstituted spinach photosystem II was studied using polarized X-ray absorption spectroscopy of oriented PS II preparations to investigate the structural and functional role of the Ca^{2+} ion in the Mn_4O_5Ca cluster of the oxygen-evolving complex (OEC). Samples were prepared by low pH/citrate treatment as one-dimensionally ordered membrane layers and poised in the Ca^{2+}-depleted S_1 (S_1') and S_2 (S_2') states, the $S_2'Y_Z^{\bullet}$ state, at which point the catalytic cycle of water oxidation is inhibited, and the Ca^{2+}-reconstituted S_1 state. Polarized Mn K-edge XANES and EXAFS spectra exhibit pronounced dichroism. Polarized EXAFS data of all states of Ca^{2+}-depleted PS II investigated show only minor changes in distances and orientations of the Mn–Mn vectors compared to the Ca^{2+}-containing OEC, which may be attributed to some loss of rigidity of the core structure. Thus, removal of the Ca^{2+} ion does not lead to fundamental distortion or rearrangement of the tetranuclear Mn cluster, which indicates that the Ca^{2+} ion in the OEC is not critical for structural maintenance of the cluster, at least in the S_1 and S_2 states, but fulfills a crucial catalytic function in the mechanism of the water oxidation reaction. On the basis of this structural information, reasons for the inhibitory effect of Ca^{2+} removal are discussed, attributing to the Ca^{2+} ion a fundamental role in organizing the surrounding (substrate) water framework and in proton-coupled electron transfer to $Y_Z^{\bullet}$ (D1-Tyr161).

Graphical abstract

[*]Corresponding Authors: vkyachandra@lbl.gov. Tel: +1 510 486 4963. jyano@lbl.gov. Tel: +1 510 486 4366.
[†]Present Address: Max-Planck-Institut für Chemische Energiekonversion, D-45470 Mülheim an der Ruhr, Germany
[‡]Present Address: Department of Chemistry, Northwestern University, Evanston, IL 60208, United States
[§]Present Address: Howard Hughes Medical Institute Janelia Research Campus, Ashburn, VA 20147, United States

Supporting Information: Comparison of Ca^{2+}-depletion methods, EXAFS equation, determination of the mosaic spread, relative MLS intensities of native, Ca^{2+}-depleted, and Ca^{2+}-reconstituted PS II, angular-dependent EPR Signal II spectra from $Y_D^{\bullet}$, isotropic Mn K-edge XANES spectra with second derivatives, and isotropic Mn K-edge EXAFS Fourier Transforms. The Supporting Information is available free of charge on the ACS Publications website at DOI: 10.1021/acs.jpcb.5b03559.

Notes: The authors declare no competing financial interest.

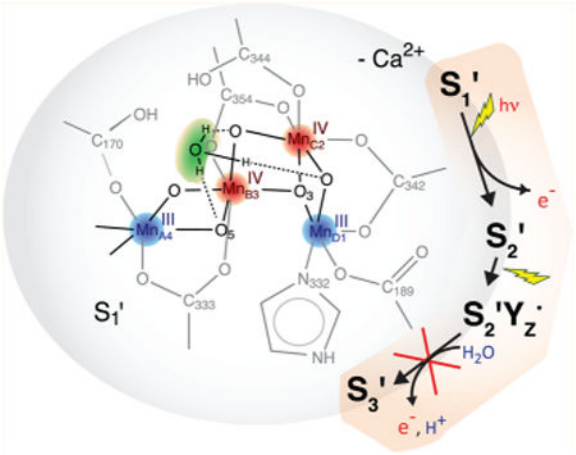

1. Introduction

A fundamental reaction in oxygenic photosynthesis is the light-driven oxidation of water, which takes place at photosystem II (PS II), an integral membrane protein complex.[1–4] The water splitting reaction is catalyzed by the oxygen-evolving complex (OEC), a lumenal protein-bound cluster containing four Mn and one Ca atom that are bridged by oxo/hydroxo-groups (Mn_4O_5Ca, Figure 1A). During the catalytic reaction, the complex undergoes successive advancement through five redox states, S_0 to S_4, before the spontaneous return to S_0, resulting in the release of O_2 (Figure 1A).[5,6] The S-state cycle of the OEC couples the one-electron photo-oxidation of the chlorophyll P_{680} in the PS II reaction center to the four-electron chemistry of water oxidation occurring at the Mn_4O_5Ca cluster. Electron transfer from the Mn_4O_5Ca cluster to $P_{680}^{\bullet+}$ proceeds via the redox-active tyrosine Y_Z (D1-Tyr161).

The general consensus is that a valence configuration of $Mn^{III}_2Mn^{IV}_2$ for the dark-stable S_1 state and $Mn^{III}Mn^{IV}_3$ for S_2 are consistent with spectroscopic and structural data and theoretical calculations.[8–14] The structure of the OEC has been investigated using X-ray diffraction (XRD) and a variety of spectroscopic methods. Crystal structures of PS II at resolutions of up to 1.9 Å[7,15–17] confirmed the presence of one Ca^{2+} ion, as had been shown previously by extended X-ray absorption fine structure (EXAFS) spectroscopy[18–23] and electron paramagnetic resonance (EPR) spectroscopy.[24–27] At present, the recent X-ray free-electron laser (XFEL) structure of PS II at 100 K provides a radiation-damage-free structure of the native resting state at a resolution of 1.95 Å.[7] To understand the catalytic mechanism, however, knowledge of the chemical nature of the Mn_4O_5Ca cluster, including the Ca^{2+} binding mode, as PS II advances through the S-state cycle is required. X-ray absorption spectroscopy (XAS), which requires much lower X-ray dose than XRD,[28] using synchrotron radiation at cryogenic temperatures allows us to study catalytic intermediates of the reaction under the threshold of radiation-induced changes and can provide higher-resolution distance information on the local environment of the metal ions.[23,29–31]

Polarized Mn EXAFS of PS II in oriented thylakoid membranes extracted from spinach yields detailed information about neighboring atoms of the four Mn atoms. Combined with a range-extended EXAFS method, polarized spectra demonstrated that in the S_1 state, there

are three di-μ-oxo bridged Mn-(μ-O)$_2$-Mn vectors, two at ∼2.7 Å (Mn_{B3}-Mn_{C2} and Mn_{C2}-Mn_{D1})[7] and one at ∼2.8 Å (Mn_{A4}-Mn_{B3})[7] distance, at an average orientation of ∼60° relative to the membrane normal.[30] Furthermore, one mono-μ-oxo bridged Mn-μ-O-Mn vector of 3.2 Å (Mn_{B3}-Mn_{D1}) aligned approximately along the membrane plane and Mn-(μ-O)$_2$-Ca vectors of ∼3.4 Å oriented approximately, on average, along the membrane normal (Mn_{B3}-Ca and Mn_{C2}-Ca)[7] were observed. Sr EXAFS of Sr^{2+}-substituted PS II[20,22] and Ca EXAFS[21] confirmed interactions of Sr and Ca with Mn at a distance of 3.5 and 3.4 Å, respectively, with an angle of 0°–23° relative to the membrane normal.[22] Moreover, a total of four Sr–Mn distances of ∼3.5 and ∼4.0 Å were found in all four accessible states, S_0 to S_3, which exhibit changes in the Mn–Mn and Ca/Sr–Mn distances, especially upon the S_2 to S_3 and S_3 to S_0 transitions.[23] Density functional theory (DFT) suggested that in the S_2 state, the OEC may exist in an equilibrium of two valence isomers, an open and a closed cubane conformation of ground spin states S = 1/2 and 5/2,[12,13,32] which give rise to a g = 2 multiline EPR signal (MLS)[33] and signals centered at $g \geq 4.1$,[34–37] respectively. It was shown that small alcohols, such as MeOH and EtOH shift the equilibrium in favor of the MLS, suppressing the $g \geq 4.1$ signals.

Ca^{2+} can be depleted from the OEC in PS II membrane preparations[38] using two different methods, which either make use of (i) high ionic strength during a salt wash, using 1–2 M NaC[39,40] or (ii) a pH drop to 3 using citric acid, which also functions as a Ca^{2+} chelator simultaneously.[41] Since the NaCl treatment suffers from some drawbacks (Section S1 of the Supporting Information), Ca^{2+} depletions in this work were carried out based on the low pH/citrate method of Ono and Inoue.[41] At pH 3, protons present at a high concentration of 1 mM neutralize negatively charged groups ligating the Ca^{2+} ion, which inhibits Ca^{2+} binding and leads to its release from the cluster. After bringing the thylakoid membranes back to physiological pH, rebinding of Ca^{2+} to the undamaged OEC is possible.

While the Ca^{2+}-depleted OEC is unable to complete the reaction cycle and oxidize water,[39–41] the resting S_1' state can be advanced to higher oxidation states via different illumination procedures.[25,26] Continuous illumination at 4 °C followed by dark-adaptation, a procedure called “annealing” in this paper, advances the OEC to the metastable S_2' state. This S = 1/2 spin state exhibits a modified MLS with more lines (at least 27) of smaller average line spacing (5.5–6 vs 8.8 mT) than in native S_2, but it does not exhibit any high-spin $g \geq 4.1$ signals (although they can be generated by near-infrared illumination).[35,36] During annealing, Ca^{2+}-depleted PS II decays rapidly to S_2' from another S_2-related state, $S_2'Y_Z^{\bullet}$, which means that the S_2' state cannot be further oxidized by the $Y_Z^{\bullet}$ radical. The interaction between the S = 1/2 spins of $Y_Z^{\bullet}$ and the S_2' state generates a split EPR signal characteristic of the $S_2'Y_Z^{\bullet}$ state, while making the S_2' signal unobservable in continuous-wave (CW) EPR. The peak-to-peak line width of this $Y_Z^{\bullet}$ split signal is ∼16 mT in spinach PS II in the presence of the extrinsic polypeptides.

A recent study of the Mn cluster in the S_2' state using EPR and ^{55}Mn electron nuclear double resonance (ENDOR)spectroscopy revealed that the Ca^{2+} ion is not critical for maintaining the electronic structure of the open-cubane conformation,[27] which exhibits the same Mn oxidation states and principal electronic exchange-coupling scheme as the native S = 1/2 S_2 state.[42–45] Thus, a role for Ca^{2+} in only tuning the redox or electronic properties of

the Mn cluster seems unlikely. While the reason for the inhibition upon removal of the Ca^{2+} ion and thus its precise function remain elusive, the following roles have also been suggested. (i) The Ca^{2+} ion could act as an (intermediate) substrate binding site.[13,17,23,46–48] (ii) The water binding function of Ca^{2+} could also be that of a "gatekeeper" for H_2O, regulating its access to the cluster and coordinating the specific binding mode to activate it.[26,49] (iii) The fact that Sr^{2+} is the only metal ion able to functionally replace Ca^{2+}[41,50,51] leads to the conclusion that their property as strong Lewis acids with similar electronegativities, giving rise to similar pK_a values of H_2O ligands, may be critical for substrate deprotonation during catalysis[52] and (iv) proton-coupled electron transfer from the OEC to $Y_Z^{\bullet}$.[52,53]

More detailed knowledge about the structure of the Ca^{2+}-depleted OEC and the effect of Ca^{2+} removal will be useful to more precisely define the ligation mode of the Ca^{2+} ion to the tetranuclear Mn cluster in catalytically relevant states of the reaction cycle and its structural and mechanistic role in photosynthetic water oxidation. Employing polarized Mn K-edge XAS on one-dimensionally ordered Ca^{2+}-depleted and Ca^{2+}-reconstituted PS II samples, the current study refines the results obtained from XAS on nonoriented samples[19] by providing angular information for Mn–Mn vectors and incorporating the latest knowledge about the OEC structure and function. In this study, the accessible Ca^{2+}-depleted states are compared, along with the untreated Mn_4O_5Ca cluster, while Ca^{2+}-reconstituted PS II serves as a control for the integrity of the samples after the Ca^{2+} depletion process and the irreversible changes, if any, that are introduced by that process.

2. Experimental Procedures

2.1. Sample Preparation

All work with isolated thylakoid membranes was performed in the dark or under dim green light, and PS II was kept at 4 °C before storage in the dark either at −80 °C or in liquid N_2. PS II-enriched thylakoid membranes were prepared from spinach by detergent treatment using Triton X-100.[38,54]

Ca^{2+} depletion and reconstitution based on the low pH/citrate treatment method[41] was achieved as described previously.[20] Before use, glassware and plasticware were acid-washed (10% HCl), and Ca^{2+}-free buffers were treated with Chelex 100 Resin to remove Ca^{2+} contamination. Untreated, Ca^{2+}-depleted and Ca^{2+}-reconstituted PS II in the final buffer (0.4 M sucrose, 50 mM 2-(*N*-4-morpholino)ethanesulfonic acid (MES), 15 mM NaCl, 5 mM $MgCl_2$, 2.5% EtOH (*v*/*v*), pH 6.5 with or without 5 mM $CaCl_2$ for Ca^{2+}-containing and Ca^{2+}-free samples, respectively) was centrifuged for 1 h at 23000*g* to obtain highly concentrated pellets.

PS II pellets were transferred to custom-built Lucite sample holders fitting both into an EPR resonator cavity and the XAS cryostat. For dark state isotropic samples (S_1' and S_1 states), the cavity of 40 μL sample holders was filled entirely, whereas for light-induced samples (S_2', $S_2'Y_Z^{\bullet}$, and S_2 states), the membranes were spread as a thin film of ∼0.5 mm on the Mylar tape backing of the sample holders. For oriented samples, to preferentially align the PS II membrane normal along the substrate normal, the membranes were painted as a very

thin and even layer on the back of the Mylar tape using a paint brush and then dried under a stream of N_2 gas for ~30 min.[55] Sufficiently thick samples for XAS measurements were generated by repeating this paint-and-dry process 6 times. All samples were dark-adapted for 1 h to accumulate the S_1' or S_1 state before freezing them for storage. S state advancement was carried out by illumination of the sample in a nonsilvered dewar from the front and the back with two tungsten lamps employing aqueous 5% $CuSO_4$ infrared filters to reduce any heating from the illumination. Illumination at 4 °C for 2 min advanced the S_1' to the $S_2'Y_Z^{\bullet}$, when samples were frozen immediately afterward,[25,26] and to the S_2' state, when samples were dark-adapted for 15–20 min at 4 °C after illumination (Figure 1B).[19] Advancement to the S_2 state to assess the Ca^{2+} content by means of MLS intensities was done by illumination of untreated, Ca^{2+}-depleted, and Ca^{2+}-reconstituted control samples at 195 K for 20 min.[26]

2.2. Oxygen Evolution Measurements

Steady-state PS II enzyme activity at 25 °C was determined by the measurement of the O_2 concentration in a PS II-containing assay mixture using a YSI 4004 Clark-type electrode (Yellow Springs Instruments) with a high sensitivity Teflon membrane under continuous illumination with a tungsten lamp through an aqueous 5% $CuSO_4$ infrared filter. The assay medium was the sample buffer lacking EtOH and with 0.4 mM 2,6-dichloro-*p*-benzoquinone (DCBQ, 50 mM in dimethyl sulfoxide) added as an electron acceptor. O_2 evolution activities were determined as an average of at least 8 single measurements at a minimum of 2 different chlorophyll concentrations ranging from 5 to 25 μg/mL.

2.3. EPR Spectroscopy

EPR spectroscopy was used for characterization and quality assurance of the samples before use in XAS studies. Every separate batch of samples was tested for damage of the OEC, Ca^{2+} content, S state composition and, for oriented samples, degree of orientation.

Low-temperature X-band CW EPR spectra at 9.28 GHz were recorded on an E-109 EPR spectrometer (Varian, Inc.) equipped with a standard TE_{102} cavity and a Helitran liquid helium cryostat (Air Products). For oriented samples, the angle between the substrate plane and the direction of the magnetic field was 0°, if not stated otherwise. A Ca^{2+}-reconstituted sample for each batch of samples was screened for the release of Mn^{II} characterized by its six-line signal, centered at $g = 2$, as an indicator of damage to the Mn_4O_5Ca cluster. The temperature was 8 K, the microwave power 0.5 mW and the modulation amplitude 32 G. None of the batches of Ca^{2+}-depleted and Ca^{2+}-reconstituted samples contained detectable amounts of Mn^{II}. In order to determine the mosaic spread Ω as a measure for the degree of disorder (Section S2 of the Supporting Information), EPR spectra of $Y_D^{\bullet}$ (D2-Tyr160) at $g = 2$ were collected from one-dimensionally ordered samples at orientations of 0° and 90° relative to the magnetic field at 20 K and 25 μW microwave power with 2.5 G modulation amplitude.[22,56] Spectra of the respective Mn_4O_5Ca cluster signals were recorded for each sample at 8 K with 30 mW microwave power and 32 G modulation amplitude. The various MLS spectra were background-corrected by light-minus-dark subtraction (i.e., the difference between the spectra after and before sample illumination).

2.4. XAS Data Collection

Mn K-edge X-ray absorption spectra were collected at Stanford Synchrotron Radiation Lightsource (SSRL) at an electron energy of 3.0 GeV and an average current of 80–100 mA on beamlines 7-3 and 9-3 using a Si(220) double crystal monochromator. These were equipped with a CF 1208 liquid helium flow cryostat (Oxford Instruments) with exchange gas (He) in the sample space to maintain a sample temperature around 10 K in order to minimize radiation damage. The intensity of the incident X-ray was monitored by an N_2-filled ion chamber (I_0) in front of the sample. The total photon flux on the sample was limited to 1×10^7 photons per μm^2, which was determined to be non-damaging on the basis of detailed radiation-damage studies of PS II solution samples.[28] Spectra were acquired by sweeping the energy of the incident X-ray beam from 6400 to 7108 eV. They were energy-calibrated with respect to the pre-edge peak of $KMnO_4$, which was placed between two N_2-filled ionization chambers (I_1 and I_2) after the sample, at 6543.3 ev[57] or PS II sample orientations of 45° and 80° toward the incident beam. For PS II sample orientations of 10°, at which no transmission signal was available, a monochromator crystal glitch at 6460.3 eV was used for energy calibration. Absorption spectra were recorded indirectly via the Mn Kα fluorescence peak using a 30-element solid-state Ge detector (Canberra Instruments) with an energy resolution of ~150 eV.

2.5. XAS Data Analysis

Energy calibration and averaging of normalized fluorescence data, weighted according to their signal-to-noise ratio, was performed using the EXAFSPAK suite of programs by Graham N. George and Ingrid J. Pickering (University of Saskatchewan). Data reduction was done using the SIXPACK program package[58] by Sam Webb (SSRL).Second derivatives of the edge spectra were obtained by a third order polynomial fit over a range of ±3 eV around each point. For the conversion of data from *E*-space to *k*-space, E_0 = 6561.3 eV was used for the Mn K-edge energy and a spline curve, fit to data above 1 $Å^{-1}$, was applied to minimize low-frequency background contributions. Fourier transforms were calculated for k^3-weighted data ranging from 3.6 to 11.2–11.9 $Å^{-1}$, truncated at zero crossings in order to minimize apodization distortions. Curve fitting to Fourier isolates back-transformed from *R* ′- to *k*-space was done according to the EXAFS eq (Section S3 of the Supporting Information) with E_0 and R_j, $N_{app,\,j}$, and σ_j for each coordination shell *j* as fitting variables, using SIXPACK. Ab initio amplitude, phase, and mean-free path functions $f_j(\pi,k,R_j)$, $\alpha_j(k)$, and $\lambda_j(k)$ were calculated using FEFF6L (University of Washington).[59] For the amplitude reduction factor S_0^2, the empirical value 0.85 from studies on model compounds was used. Relative angles φ_j of the absorber-backscatter vectors and isotropic coordination numbers $N_{iso,j}$ were obtained from the dependence of $N_{app,j}$ on the sample orientation θ between the substrate normal and the incident X-ray E-vector, given by eq 1, by fitting of the linear correlation between $N_{app,j}$ and $3\cos^2\theta$–1.

$$N_{\mathrm{app},j}(\theta)=N_{\mathrm{iso},j}+0.5N_{\mathrm{iso},j}(3\cos^2\theta-1)\times(3\cos^2\phi_j-1)-I_{\mathrm{ord}}(\Omega) \quad (1)$$

The order integral I_{ord} is defined by the mosaic spread Ω as

$$I_{\mathrm{ord}}(\Omega)=0.5\frac{\int_0^{\pi/2}\sin\alpha\times(3\cos^2\alpha-1)\times\exp(-\alpha^2\ln 2/\Omega)d\alpha}{\int_0^{\pi/2}\sin\alpha\times\exp(-\alpha^2\ln 2/\Omega)d\alpha} \quad (2)$$

A more detailed description of polarized EXAFS can be found in refs 22 and 30.

3. Results

3.1. Sample Characterization

We prepared PS II samples in four well-defined states, Ca^{2+}-depleted S_1', S_2', $S_2'Y_Z^{\bullet}$, and Ca^{2+}-reconstituted S_1 (Figure 1). The O_2 evolution activities were measured for native, Ca^{2+}-depleted, and Ca^{2+}-reconstituted samples to ensure sample integrity and quantify the degree of Ca^{2+} depletion. Because the Ca^{2+}-depleted OEC fraction cannot complete the S-state cycle and therefore does not evolve oxygen, the O_2 activity serves as a measure for the fraction of Ca^{2+}-containing metal clusters in the sample and, thus, for the degree of Ca^{2+} depletion and reconstitution. The degree of reconstitution is an indicator for the integrity of the samples, since irreversible damage of the PS II complex as a result of the treatment with citric acid at low pH can prevent the restoration of O_2 evolution activity. The O_2 evolution rates of different sample preparations were 340–400 μmol O_2/mg Chl/h for native, 50–80 μmol O_2/mg Chl/h for Ca^{2+}-depleted, and 250–300 μmol O_2/mg Chl/h for Ca^{2+}-reconstituted samples. This corresponds to ∼82% Ca^{2+}-free Mn clusters in the Ca^{2+}-depleted PS II samples on average, out of which ∼69% could be reconstituted by the addition of Ca^{2+}.

The degrees of Ca^{2+} depletion and Ca^{2+} reconstitution were evaluated also on the basis of the S_2 state MLS arising from the fraction of Ca^{2+}-containing OEC upon illumination at 195 K. At this temperature, the Ca^{2+}-free metal cluster in the S_1' state, which exhibits no X-band perpendicular-mode EPR signal, cannot be advanced to any other oxidation state.[26] The relative MLS intensities in light-minus-dark difference spectra of untreated, Ca^{2+}-depleted and Ca^{2+}-reconstituted PS II samples normalized to the $Y_D^{\bullet}$ signal confirmed Ca^{2+} depletion and reconstitution (Figure S1 of the Supporting Information).

Advancement of Ca^{2+}-depleted samples from S_1' to the designated higher oxidized states upon illumination at 4 °C was confirmed by the presence of their characteristic EPR signals, the S_2' altered MLS, and the $S_2'Y_Z^{\bullet}$ split signal (Figure 2, middle and bottom, respectively). We note that these spectra also show signals from smaller fractions of other states (consistent with the O_2 assays); the $S_2'Y_Z^{\bullet}$ sample (not dark-adapted) exhibits residual S_2 state MLS (compare Figure 2, top) from the Ca^{2+}-containing PS II fraction, and the S_2' spectrum contains traces of the $S_2'Y_Z^{\bullet}$ split signal. The yield of S_2' state cannot be reliably quantified from the modified MLS spectra. Comparison to spectra from S_2' state samples generated in the presence of DCMU[19,27] (see Figure 1B) and the known lowered inflection point energy of the Mn K-edge upon annealing[19] (see sections 3.2 and 4.1.1), however, suggest that further reduced S_1' or even S_0' states may be present besides S_2'.

For the polarized XAS experiments, one-dimensionally ordered PS II samples in each of the four different states of the OEC investigated were prepared, in addition to randomly oriented

ones. The mosaic spread Ω values of the ordered membrane layers were evaluated by means of the orientation-dependent EPR signal of the oxidized $Y_D^{\bullet}$ radical (Figure S2 of the Supporting Information). For a detailed explanation of the evaluation of orientational disorder within the samples, see section S2 of the Supporting Information. The dichroic ratio of the oriented samples used for XAS experiments ranged from 3.3 to 5.3 with an average of 3.9 ± 0.6. According to the calibration curve of Andrews,[56] which relates the dichroic ratio to Ω via the angular dependence of the cytochrome b_{559} EPR signal, the mosaic spread was found to be 15–20°. For evaluation of the angle dependence of the apparent coordination numbers $N_{app,j}$, derived from polarized EXAFS data (sections 2.5 and 3.5),[30] the lower limit of 20° was chosen.

3.2. Polarized XANES

Polarized Mn K-edge XANES spectra of the oriented samples poised in the three Ca^{2+}-depleted states S_1', S_2', and $S_2'Y_Z^{\bullet}$, and the Ca^{2+}-reconstituted S_1 state at angles θ of 10° and 80° between the sample normal and the X-ray E-vector are shown in Figure 3 together with the second derivatives. The spectrum of an anisotropic sample collected at the magic angle of ∼54.7°, where the angular-dependent term in eq 1 becomes zero, is identical with the isotropic spectrum of a nonoriented sample. Taking into account the angular dependence of the absorption coefficient $\mu(E) \propto 3\cos^2\theta - 1$, the isotropic spectrum can be calculated from two polarized spectra measured at different angles θ. The isotropic spectra calculated from the 10° and 80° polarized data are consistent with the spectra obtained from nonordered samples (Figure S3 of the Supporting Information). As Mn K-edge XANES is a direct probe of the electronic structure of the metal complex, this shows that the Ca^{2+}-depleted and Ca^{2+}-reconstituted OEC is not perturbed by the layering procedure. The isotropic XANES spectra of the different states are compared in Figure 4.

The inflection point energy (IPE) of the Mn K-edge was extracted from the zero crossing of the second derivative in the energy region between 6550 and 6554 eV (bottom of Figures 3 and 4 and Figure S3 of the Supporting Information). IPE values for the different states from oriented (10°, 80°) and nonoriented (54.7°) samples (the numbers of which are shown in parentheses) are listed in Table 1. The isotropic values in the last column were calculated by linear fits from the three orientations. The IPE of the $S_2Y_Z^{\bullet}$ state, made by illumination of the S_1' state at 4 °C, was shifted to a higher energy by ∼1 eV from that of S_1'. In contrast, the S_2' state made by dark adaptation of the $S_2'Y_Z^{\bullet}$ state at 4 °C has a lower IPE than those of S_1' and the S_2' state generated by illumination in the presence of DCMU (see Discussion section 4.1.1).[19] As in the native S_1[29,30,61] and S_2 states,[29] the dichroism of the spectra is expressed by a higher IPE at 80° compared to 10° in all four cases, with the IPE difference ranging from 0.6 eV in S_1' state samples to 1.7 eV in $S_2'Y_Z^{\bullet}$ state samples.

3.3. Polarized EXAFS

k^3-Weighted Mn K-edge EXAFS spectra and their Fourier transforms for one-dimensionally oriented samples measured at orientations θ of 10° and 80° in the series of Ca^{2+}-depleted and Ca^{2+}-reconstituted states are shown in Figure 5. The apparent distance R' is shorter than the actual distance due to a phase shift induced by the interaction of the respective absorber-backscatterer pair with the photoelectron. The isotropic Fourier transforms calculated from

the 10° and 80° polarized data are highly similar to the spectra obtained from isotropic solution samples (Figure S4 of the Supporting Information), confirming structural integrity of the OEC in oriented Ca^{2+}-depleted and -reconstituted samples.

For all states, EXAFS data show clear angular dependence. All Fourier transforms exhibit the same general appearance of three peaks I, II, and III, characteristic for the OEC. Peaks I and II correspond to Mn–O and Mn–N interactions at 1.8–2.0 Å and Mn-(μO)$_2$-Mn interactions at 2.7–2.8 Å, respectively. These peaks are higher in amplitude at $\theta = 80°$ compared to $\theta = 10°$, as also observed for one-dimensionally oriented native samples.[29,30,61] In the Ca^{2+} -reconstituted OEC, peak III is more intense at 10° than at 80°, similar to the native Mn_4O_5Ca cluster in the S_1 and S_2 states, albeit less dichroic.[29] In the native Mn_4O_5Ca cluster, Mn-μO-Mn and Mn-(μO)$_2$-Ca interactions at ∼3.3 Å give rise to peak III.[18-23] Due to the lack of Mn–Ca interactions, this peak has a smaller amplitude for the Ca^{2+}-depleted states than for the Ca^{2+}-reconstituted state, as has been reported before for isotropic samples.[19] Also, peak II in the Ca^{2+}-reconstituted OEC is found to be larger in amplitude than in the Ca^{2+}-depleted states. Overall, no major spectral changes are observed between the Ca^{2+}-depleted and reconstituted samples, indicating that the spatial arrangement of the tetranuclear Mn cluster remains the same.

3.4. EXAFS Curve Fitting

In order to extract quantitative information from the Mn K-edge EXAFS spectra describing the local structure of the OEC in the investigated states and to reveal subtle differences between them, curve fitting to Fourier isolates (0.9 Å < R' < 3.5 Å) in k-space was performed. Features at $R' > 3.5$ Å and $R' < \sim 1$ Å, which result from high-frequency noise components in the k-space spectrum and imperfect background removal respectively, are filtered out by Fourier isolation. As in previous studies of the native[29] as well as theCa^{2+}-depleted[29] OEC, the same three major paths corresponding to the individual peaks were used for the fits. For the Ca^{2+}-containing S_1 state, the Mn-(μO)$_2$-Ca interactions contributing to peak III were not explicitly considered.[19,29] The Debye–Waller factors σ_j, which are highly correlated to the coordination number N_j, were fixed to reasonable numbers chosen empirically based on previous studies[18,19,23,29–31] in order to compare the N_j values and thus the number of interactions in the different states and determine their orientations. SIXPACK returns the fit error parameters χ and χ^2, the latter of which takes into account the number of fit variables and independent data points. Absolute fit quality was chosen based on a combination of criteria, which include the above parameters and physical and chemical feasibility of the resulting parameters.

Curve fitting of k-space data of an oriented and a nonoriented S_1' state sample are shown in Figure 6. All averaged absorber-backscatterer distances R_j and apparent coordination numbers $N_{\mathrm{app},j}$ from fits to Fourier isolates are reported in Table 2. It can be seen that the EXAFS spectra of Ca^{2+}-depleted samples can be fit well without incorporation of a Mn–Ca interaction, whereas this interaction needs to be accounted for in the Ca^{2+}-reconstituted samples. The coordination numbers found reflect the dichroism seen in the EXAFS spectra.

3.5. Determination of $N_{iso,j}$ and ϕ_j

The apparent coordination numbers N_{app} at different measurement angles θ depend on the angle φ of the absorber-backscatterer vector toward the membrane normal as given in eq 1. In order to obtain angular information for individual shells and the averaged isotropic coordination number $N_{iso,j}$, we carried out linear regression analysis of $N_{app,j}$ with respect to θ. For all fits, the approximate average mosaic spread Ω of 20° assessed by EPR measurements was used.

Figure 7 shows linear plots in which the experimental $N_{app,j}$ values are plotted against 3 $\cos^2 \theta - 1$. The ordinate intercepts of the linear fits correspond to N_{iso}, while the slope contains contributions from both N_{iso} and φ. Table 3 lists $N_{iso,j}$ and φ_j from the linear regression analysis, as well as distances R_j of the backscattering atoms in the various states investigated, averaged over the samples of all orientations. Additionally, numbers for the native OEC in the S_1 state[30] reported previously are listed for comparison.

4. Discussion

We have studied the structural role of Ca^{2+} in the OEC using XAS by comparing the Ca^{2+}-depleted and Ca^{2+}-reconstituted samples. Previous studies by several groups including ours have reported that Ca^{2+} is a critical element for the catalytic activity of the OEC; without Ca^{2+}, the S_2 to S_3 transition is blocked and Ca^{2+}-depleted PS II loses its ability to evolve O_2.[19,25–27] The enzymatic activity can be mostly recovered by adding Ca^{2+} to the Ca^{2+}-depleted samples.[39–41] To date, the precise reason for this inhibition in the absence of Ca^{2+} has still not been identified. While this study also does not provide a final answer to this question, the structural analysis of the Ca^{2+}-depleted and Ca^{2+}-reconstituted OEC on the basis of interatomic distances and binding angles in the following is able to rule out possible roles of Ca^{2+} in photosynthetic water oxidation.

4.1. Effects of Ca^{2+} Depletion and Reconstitution on Structure and S′-State Transitions

4.1.1. Mn Oxidation States—The IPE of an X-ray absorption K-edge indicates the difference between the ionization threshold and the 1s orbital energy. Thus, it is generally sensitive to the charge density at the absorber atom, which is most affected by the formal oxidation state. The Mn K-edge XANES spectra of the Ca^{2+}-depleted S_1' state and the Ca^{2+}-reconstituted S_1 state show similar rising edge positions and spectral features (Figure 3, panels A and D, and Figure S3, panels A and D, of the Supporting Information), with IPE values of 6551.5 ± 0.2 eV and 6551.6 ± 0.2 eV, respectively. The large variation in the IPE of the native S_1 state in the literature (6551.5 ± 1.2 eV),[8,10,31,62–69] which arises mostly because of the different data processing methods used, makes a comparison difficult. However, the Ca^{2+}-depleted S_1' and Ca^{2+}-reconstituted S_1 state IPE values, matching the untreated S_1 IPEs reported by our group using the same method, indicate that the overall Mn oxidation state, assigned as $Mn^{III}_2Mn^{IV}_2$ for the S_1 state,[8–11,13,14] remains unchanged by Ca^{2+} depletion and reconstitution. This is in line with the EPR/^{55}Mn ENDOR-spectroscopic analysis of the Ca^{2+}-depleted S_2' state,[27] which reveals the same Mn valence state distribution as in the native S_2 state, $Mn_{D1}{}^{IV}Mn_{C2}{}^{IV}Mn_{B3}{}^{IV}Mn_{A4}{}^{III}$. While identical IPEs for the native and Ca^{2+}-reconstituted S_1 states have been observed in this as well as some of

the previous studies,[18,70] we note that two studies reported 0.4–0.8 eV lower edge positions for S_1' compared to Ca^{2+}-containing S_1 states.[68,70] We think this discrepancy may result from different methods used in these previous studies, namely the use of half-height energies instead of IPEs[70] and Ca^{2+}-depletion by a NaCl salt wash,[68] which could potentially destabilize the OEC by washing out some of the extrinsic polypeptides. With regard to S′-state advancement of the Ca^{2+}-depleted OEC (Figure 1B), we observed a phenomenology described before: (i) The IPE of the $S_2'Y_Z^{\bullet}$ state is markedly higher than that of the S_1' state (1.1 eV), consistent with oxidation of the Mn atoms during transition from S_1' to $S_2'Y_Z^{\bullet}$.[19,68,71,72] (ii) The IPE of S_2' state samples, generated by annealing of the $S_2'Y_Z^{\bullet}$ state, is ∼0.7 eV below the edge position of the S_1' state despite the one-electron oxidation, suggesting a modification of the electronic state during the dark-adaptation. This may indicate vulnerability to reduction of the Ca^{2+}-free tetra-Mn complex as proposed before,[19] even over the rather short times used for dark adaptation (15–20 min). The following findings suggest a relatively slow Mn reduction process in annealed S_2' by a reductant accumulating during illumination of the inhibited PS II to be the cause: (i) After shorter annealing times (5–10 instead of 15–20 min), a considerably larger IPE lying between the S_1' and the $S_2'Y_Z^{\bullet}$ state has been measured.[68] (ii) When the S_1' state is advanced to the S_2' state in the presence of DCMU[19,70] or by one laser flash,[71] in both cases without a subsequent annealing step, the IPE is higher than that of the S_1' state but slightly lower than that of $S_2'Y_Z^{\bullet}$. It is noted that there are neither indications of Mn^{II} (EPR, XANES[19]) nor of considerable structural changes in the EXAFS, such as Mn-O and Mn-Mn distance elongations characteristic of Mn^{II} formation.[28,73] Additionally, no intensity changes were observed in the pre-edge region in the Ca^{2+}-depleted and -reconstituted states (Figure 3 and Figure S3 of the Supporting Information), suggesting that no symmetry changes occur in their Mn ligand spheres.

4.1.2. Geometric Structure—In order to interpret the coordination numbers $N_{iso,j}$ in a multinuclear system in terms of the number of absorber-backscatterer interactions I_j in one shell j, the total number of absorbing atoms A in the system and the number of absorbers B_j in the respective shell have to be considered according to eq 3:

$$N_{iso,j} = I_j \times B_j / A \quad (3)$$

To determine I_j in the various shells for OEC, the values of $N_{iso,j}$ from the fits have to be normalized by the four Mn atoms (by multiplication with $A = 4$). For interactions involving two absorbing atoms (i.e., for the Mn–Mn shells), they additionally have to be divided by $B = 2$.

Due to the strong correlation with the Debye–Waller factors, which are rather flexible over a certain range, and the large number of interactions in shell 1, their N_{iso} and absorber-backscatter angle φ_j cannot be interpreted quantitatively on this basis. However, by keeping σ_j constant under the assumption of a similar degree of distance disorder, N_{iso} can be compared for different states of the OEC (Table 3). The Ca^{2+}-reconstituted S_1 and the Ca^{2+}-depleted S_1' and S_2' states exhibit a similar N_{iso} of 2.6–2.7, indicating no changes in Mn coordination spheres and identical numbers of Mn–O/N ligands. The small increase in the

intensity of peak I in the $S_2'Y_Z^{\bullet}$ state (Figure 5B, see also ref 72) results in a slightly larger N_{iso} of 3.1. This increase in intensity could be interpreted as an additional ligand to Mn in the $S_2'Y_Z^{\bullet}$ state. Another possible interpretation is a more uniform distribution of Mn-ligand distances in the interactions contributing to this Fourier peak in the $S_2'Y_Z^{\bullet}$ state if σ_j is not constant.

All four states investigated exhibit coordination numbers of ∼1.2 for shell two, similar to the native OEC (Table 3, refs 29 and 30). Thus, the peak II region, with an N_{iso} systematically smaller than 1.5, can be explained by three Mn-(μO)$_2$-Mn interactions at average distances between 2.7 and 2.8 Å: Mn_{A4}-Mn_{B3}, Mn_{B3}-Mn_{C2}, and Mn_{C2}-Mn_{D1}.[7,13,32,74–76] While it also can be simulated by two shorter (∼2.7 Å) and one longer (2.8–2.9 Å) Mn-(μO)$_2$-Mn distances (not shown) as in native S_1 and S_2,[30,77] this arrangement cannot be proven for the Ca^{2+}-depleted and reconstituted OECs due to the resolution limit of non-range-extended EXAFS. In terms of the peak III region, the coordination numbers in the Ca^{2+}-depleted OEC are consistently lower than in the Ca^{2+}-containing Mn_4O_5Ca clusters, immediately reflecting the absence of the Mn–Ca interactions and thus the absence of the Ca^{2+} ion in the Ca^{2+}-depleted samples. The N_{iso} = 0.2–0.3 in the S′ states arises from a long Mn–Mn interaction around 3.3 Å,[19] which is most likely the Mn_{B3}-μO-Mn_{D1} interaction (Figure 8).[7,13,32,74–76] The dominating contribution from peaks I and II in the *k*-space spectra, as well as the lower signal-to-noise level of peak III, lead to numbers smaller than expected. By comparison with both conventional and range-extended EXAFS on the native OEC previously reported by our group,[29,30] we conclude that there are also at least two Mn-(μO)$_2$-Ca interactions at ∼3.3 Å in the Ca^{2+}-reconstituted S_1 state. Coordination numbers and distances for the S′ states are in good agreement with recent DFT-based structures of the Ca^{2+}-depleted OEC.[74–76]

In terms of distances and angles, no fundamental rearrangement of atoms upon Ca^{2+} removal or reinsertion is found in any of the investigated states (Table 3). However, small changes of internuclear distances seem to accompany these processes. Most pronounced is the lengthening of the Mn_{B3}-μO-Mn_{D1} interaction in peak III from 3.20 Å in native S_1[30] to ∼3.3 Å upon Ca^{2+} depletion. The superposition of interactions in the small peak III of the Ca^{2+}-containing OEC does not allow for interpretation of the exact distances and angles of the shell 3 fit to conventional EXAFS data. For all states, the other distances are highly similar to the native S_1 state (see also ref 11). Small elongations (0.02 Å) of distances in all shells seem to occur during the advancement of the Ca^{2+}-depleted OEC to the $S_2'Y_Z^{\bullet}$ state. Evaluation of the dichroism in the polarized EXAFS spectra shows basically no changes in the angles (∼60°) of the Mn-(μO)$_2$-Mn vectors of shell 2 relative to the membrane normal, and are consistent with the ones found in the native S_1 and S_2 states.[29,30] The fact that their orientations are constant throughout all of the states investigated (S_1 and S_1', S_2 and S_2', or $S_2'Y_Z^{\bullet}$) is in agreement with the above discussion of the interatomic distances and shows that only minor structural changes occur in the Ca^{2+}-depleted OEC, as also suggested by recent computational models.[74–76]

Altogether, Ca^{2+} depletion neither led to release of Mn from the cluster nor to a change in Mn oxidation states, Mn coordination geometries or the stoichiometry of Mn–Mn interactions in the individual ligand shells, or to rebinding of backscatterer atoms in place of

the Ca^{2+} ion. The impact of the removal of the Ca^{2+} ion from the OEC is not an immediate distortion of the metal complex but rather leads to a marginal loosening of the cluster, evident from the increase (<0.1 Å) of the longest Mn–Mn distance, constituting peak III. Thus, Ca^{2+} removal slightly destabilizes the cuboidal core structure, likely affecting the Mn_{B3}-μO-Mn_{D1} interaction. This provides a rationale for the fact that the Ca^{2+}-depleted OEC in the S_2' state does only adopt the low-spin, proposed open-cubane conformation,[12,13] as apparent from its EPR spectrum, featuring the altered $S = 1/2$ MLS but lacking the $g = 4.1$ signal with a proposed closed-cubane conformation. The Ca^{2+} ion can be rationalized as a requirement for maintaining the contracted, closed cubane of the high-spin conformation with a shorter Mn_{B3}-Mn_{D1} distance of ~2.9 Å,[12,13,32] or for advancement to an S_3 state, where a closed cubane-like structure has been proposed from EXAFS studies of native PS II.[31]

4.2. Role of the Ca^{2+} Ion in Photosynthetic Water Oxidation

The EXAFS results show that the Ca^{2+} ion is not replaced by other metal ions. Instead, loss of the Ca^{2+} ion is probably compensated by the binding of protons[75] and/or hydroxonium ions (Figure 8). The structural changes in distances, angles, and coordination numbers observed for the Ca^{2+}-depleted S′ states reflect some loosening of the tetranuclear Mn complex. The retention of structural integrity in the Ca^{2+}-depleted Mn cluster is the prerequisite that the Ca^{2+} ion can be exchanged and that reconstitution can reactivate the catalyst. Thus, the oxygen-bridged tetranuclear Mn open-cubane structure possesses an inherent stability even in the absence of the Ca^{2+} ion. Its nondestructive removal demonstrates that Ca^{2+} is not strongly bound to the cluster. This could be a consequence of some structural flexibility of the Mn_4O_5Ca cluster, as also seen in the S_2 state, in which the O5 ligand (Figure 1) of Ca^{2+} has been proposed to switch between two positions.[12,13] This is consistent with the observation that Ca^{2+} depletion is facilitated under illumination.[24,78] In the native S_2 state, the Ca^{2+} exhibits a more asymmetric, distorted ligand geometry in the open than in the closed conformation.[12] Stabilization of the Ca^{2+} coordination sphere by increasing its symmetry would then contribute to the low energy of the closed structure, only 1 kcal mol^{-1} higher than the open one. As there is no such energetic gain in the absence of the Ca^{2+} ion, the open cubane is energetically favored over the closed form in the Ca^{2+}-depleted S_2' state.

Lately, a number of theoretical studies investigated the nature of the $S_2Y_Z^{\bullet}$ state, with varying outcomes.[13,48,53,79] Very recently, the first pulsed EPR-spectroscopic study of the OEC in the S_3 state suggested in combination with DFT computations that the cluster is in an open-cubane Mn^{IV}_4 state with an additional hydroxide bound to the hexacoordinate Mn_{D1}.[80] The group of Guidoni proposed the S_2-to-S_3 transition to proceed via a closed-cubane structure in the $S_2Y_Z^{\bullet}$ state[48,79] (see also ref 13), which could be envisaged as a rationale for the inhibition of the Ca^{2+}-depleted OEC at this stage, unable to advance to an S_3' state. However, the absence of a corresponding split signal in native PS II preparations involving the high-spin $g = 4.1$ signal (see refs 53 and 79) and lack of a pathway that describes the (back-)conversion of the closed ($S_2Y_Z^{\bullet}$) into the open (S_3) conformation leaves this question unresolved at this point.

Previous EXAFS studies[11,23,31] showed that the formation of the S_3 state is accompanied by structural changes of the cluster, which involves an elongation of Mn–Mn distances, specifically one of the shorter Mn–Mn interactions of ∼2.8 Å, albeit not of the Mn–Ca vectors. Since such a displacement would likely not be impeded in the less rigid Ca^{2+}-depleted OEC, the role of the Ca^{2+} ion in this transition could instead be the ordering of the nearby water matrix/H-bonding network. Such a possibility includes (i) an involvement in coordination and transfer of the second (late binding) substrate to Mn_{A4}, as suggested in refs 13 and 48 or Mn_{D1}, see refs 80–82, by (a) direct substrate binding [e.g., W3 (Figure 1)], (b) positioning/directing a substrate coming from the bulk matrix, and/or (c) facilitating deprotonation to yield OH^-.[13,51,52] The Lewis acidity of Ca^{2+} and the correlation of proposed H^+ release and Ca^{2+}-dependence of the individual S-state transitions suggest that the H^+ could indeed come from a Ca^{2+}-bound H_2O.[83] (ii) It could act as a gatekeeper, restricting access of water to the Mn open coordination site at too early a stage of the cycle,[26,49] timing its binding exactly after reduction of $Y_Z^\bullet$. The similar spectral changes during advancement to the S_3 and the $S_2'Y_Z^\bullet$ state [i.e., the Mn–Mn distance elongations (Table 3 and refs 11 and 23)] could be a result of water binding in $S_2'Y_Z^\bullet$, arrested in an energetically stabilized configuration. On the other hand, the resulting coordination of the water ligand to Mn^{III} instead of Mn^{IV} makes this seem less likely. (iii) A crucial role of the Ca^{2+} ion in proton-coupled electron transfer from the OEC to the $Y_Z^\bullet$ residue is strongly supported by recent studies.[52,53,74,76] (iv) A direct adverse effect of Ca^{2+} depletion on the oxidation of Mn_{D1} during the S_2'-to-S_3' transition has recently been put forward in theoretical studies.[75,76] (v) Experimental[45,82,84] and computational[85] evidence that the first (early binding), slowly exchanging substrate is O5 suggests that the Lewis acidity of the Ca^{2+} ion may also be critical for providing the specific electropositive environment for this ligand discussed above. Withdrawing electron density from O5 could make it susceptible to a nucleophilic attack or to direct oxidation conferring radical character to it.

Understanding the function of the Ca^{2+} ion in photosynthetic water oxidation is highly important as it is linked to several critical steps in the mechanism of catalysis. This study shows that this role is not so much the provision of a structural framework of the tetranuclear Mn complex itself, at least in the S_1 and S_2 states, but rather to fulfill a distinct catalytic task, for example by organizing the functionally critical water environment. Further knowledge about the details of this process is necessary to fully understand the way nature converts solar energy into a chemical form and could help to find a way to make improved usage of the sun as our primary energy source.

Supplementary Material

Refer to Web version on PubMed Central for supplementary material.

Acknowledgments

This work was supported by the NIH Grant GM 55302, and by the Director, Office of Science, Office of Basic Energy Sciences (OBES), Division of Chemical Sciences, Geosciences, and Biosciences of the Department of Energy (DOE) under Contract DE-AC02-05CH11231. This work was performed at SSRL, which is funded by the DOE Office of Basic Energy Science. The SSRL SMB Program is supported by the NIH National Center for Research Resources, Biomedical Technology Program, and by the DOE Office of Biological and Environmental Research.

References

1. Nelson N, Yocum CF. Structure and Function of Photosystems I and II. Annu Rev Plant Biol. 2006; 57:521–565. [PubMed: 16669773]
2. Vinyard DJ, Ananyev GM, Dismukes GC. Photosystem II: The Reaction Center of Oxygenic Photosynthesis. Annu Rev Biochem. 2013; 82:577–606. [PubMed: 23527694]
3. Cox N, Pantazis DA, Neese F, Lubitz W. Biological Water Oxidation. Acc Chem Res. 2013; 46:1588–1596. [PubMed: 23506074]
4. Yano J, Yachandra V. Mn_4Ca cluster in Photosynthesis: Where and How Water is Oxidized to Dioxygen. Chem Rev. 2014; 114:4175–4205. [PubMed: 24684576]
5. Joliot P, Barbieri G, Chabaud R. A New Model of Photochemical Centers in System II. Photochem Photobiol. 1969; 10:309–329.
6. Kok B, Forbush B, McGloin M. Cooperation of Charges in Photosynthetic O_2 Evolution-1. A Linear Four Step Mechanism. Photochem Photobiol. 1970; 11:457–475. [PubMed: 5456273]
7. Suga M, Akita F, Hirata K, Ueno G, Murakami H, Nakajima Y, Shimizu T, Yamashita K, Yamamoto M, Ago H, et al. Native Structure of Photosystem II at 1.95 Å Resolution Viewed by Femtosecond X-ray Pulses. Nature. 2015; 517:99–103. [PubMed: 25470056]
8. Roelofs TA, Liang W, Latimer MJ, Cinco RM, Rompel A, Andrews JC, Sauer K, Yachandra VK, Klein MP. Oxidation States of the Manganese Cluster during the Flash-induced S-state Cycle of the Photosynthetic Oxygen-evolving Complex. Proc Natl Acad Sci USA. 1996; 93:3335–3340. [PubMed: 11607649]
9. Bergmann U, Grush MM, Horne CR, DeMarois P, Penner-Hahn JE, Yocum CF, Wright DW, Dube CE, Armstrong WH, Christou G, et al. Characterization of the Mn Oxidation States in Photosystem II by Kβ X-ray Fluorescence Spectroscopy. J Phys Chem B. 1998; 102:8350–8352.
10. Messinger J, Robblee JH, Bergmann U, Fernandez C, Glatzel P, Visser H, Cinco RM, McFarlane KL, Bellacchio E, Pizarro SA, et al. Absence of Mn-Centered Oxidation in the $S_2 \rightarrow S_3$ Transition: Implications for the Mechanism of Photosynthetic Water Oxidation. J Am Chem Soc. 2001; 123:7804–7820. [PubMed: 11493054]
11. Haumann M, Muller C, Liebisch P, Iuzzolino L, Dittmer J, Grabolle M, Neisius T, Meyer-Klaucke W, Dau H. Structural and Oxidation State Changes of the Photosystem II Manganese Complex in Four Transitions of the Water Oxidation Cycle ($S_0 \rightarrow S_1$, $S_1 \rightarrow S_2$, $S_2 \rightarrow S_3$, and $S_{3,4} \rightarrow S_0$) Characterized by X-ray Absorption Spectroscopy at 20 K and Room Temperature. Biochemistry. 2005; 44:1894–1908. [PubMed: 15697215]
12. Pantazis DA, Ames W, Cox N, Lubitz W, Neese F. Two Interconvertible Structures that Explain the Spectroscopic Properties of the Oxygen-Evolving Complex of Photosystem II in the S_2 State. Angew Chem Int Ed. 2012; 51:9935–9940.
13. Isobe H, Shoji M, Yamanaka S, Umena Y, Kawakami K, Kamiya N, Shen JR, Yamaguchi K. Theoretical Illumination of Water-inserted Structures of the $CaMn_4O_5$ Cluster in the S_2 and S_3 States of Oxygen-evolving Complex of Photosystem II: Full Geometry Optimizations by B3LYP Hybrid Density Functional. Dalton Trans. 2012; 41:13727–13740. [PubMed: 23037319]
14. Yano J, Yachandra VK. Oxidation State Changes of the Mn4Ca Cluster in Photosystem II. Photosynth Res. 2007; 92:289–303. [PubMed: 17429751]
15. Ferreira KN, Iverson TM, Maghlaoui K, Barber J, Iwata S. Architecture of the Photosynthetic Oxygen-evolving Center. Science. 2004; 303:1831–1838. [PubMed: 14764885]
16. Guskov A, Kern J, Gabdulkhakov A, Broser M, Zouni A, Saenger W. Cyanobacterial Photosystem II at 2.9-Å Resolution and the Role of Quinones, Lipids, Channels and Chloride. Nat Struct Mol Biol. 2009; 16:334–342. [PubMed: 19219048]
17. Umena Y, Kawakami K, Shen JR, Kamiya N. Crystal Structure of Oxygen-evolving Photosystem II at a Resolution of 1.9 Å. Nature. 2011; 473:55–60. [PubMed: 21499260]
18. Latimer MJ, DeRose VJ, Mukerji I, Yachandra VK, Sauer K, Klein MP. Evidence for the Proximity of Calcium to the Manganese Cluster of Photosystem II: Determination by X-ray Absorption Spectroscopy. Biochemistry. 1995; 34:10898–10909. [PubMed: 7662671]

19. Latimer MJ, DeRose VJ, Yachandra VK, Sauer K, Klein MP. Structural Effects of Calcium Depletion on the Manganese Cluster of Photosystem II: Determination by X-ray Absorption Spectroscopy. J Phys Chem B. 1998; 102:8257–8265. [PubMed: 25152697]
20. Cinco RM, Robblee JH, Rompel A, Fernandez C, Yachandra VK, Sauer K, Klein MP. Strontium EXAFS Reveals the Proximity of Calcium to the Manganese Cluster of Oxygen-Evolving Photosystem II. J Phys Chem B. 1998; 102:8248–8256. [PubMed: 25152698]
21. Cinco RM, Holman KLM, Robblee JH, Yano J, Pizarro SA, Bellacchio E, Sauer K, Yachandra VK. Calcium EXAFS Establishes the Mn-Ca Cluster in the Oxygen-Evolving Complex of Photosystem II. Biochemistry. 2002; 41:12928–12933. [PubMed: 12390018]
22. Cinco RM, Robblee JH, Messinger J, Fernandez C, Holman KLM, Sauer K, Yachandra VK. Orientation of Calcium in the Mn_4Ca Cluster of the Oxygen-Evolving Complex Determined Using Polarized Strontium EXAFS of Photosystem II Membranes. Biochemistry. 2004; 43:13271–13282. [PubMed: 15491134]
23. Pushkar Y, Yano J, Sauer K, Boussac A, Yachandra VK. Structural Changes in the Mn_4Ca Cluster and the Mechanism of Photosynthetic Water Splitting. Proc Natl Acad Sci U S A. 2008; 105:1879–1884. [PubMed: 18250316]
24. Boussac A, Rutherford AW. Nature of the Inhibition of the Oxygen-Evolving Enzyme of Photosystem II Induced by NaCl Washing and Reversed by the Addition of Ca^{2+} or Sr^{2+} Biochemistry. 1988; 27:3476–3483.
25. Boussac A, Zimmermann JL, Rutherford AW. EPR Signals from Modified Charge Accumulation States of the Oxygen Evolving Enzyme in Ca^{2+}-Deficient Photosystem II. Biochemistry. 1989; 28:8984–8989. [PubMed: 2557913]
26. Sivaraja M, Tso J, Dismukes GC. A Calcium-Specific Site Influences the Structure and Activity of the Manganese Cluster Responsible for Photosynthetic Water Oxidation. Biochemistry. 1989; 28:9459–9464. [PubMed: 2558720]
27. Lohmiller T, Cox N, Su JH, Messinger J, Lubitz W. The Basic Properties of the Electronic Structure of the Oxygen-evolving Complex of Photosystem II Are Not Perturbed by Ca^{2+} Removal. J Biol Chem. 2012; 287:24721–24733. [PubMed: 22549771]
28. Yano J, Kern J, Irrgang KD, Latimer MJ, Bergmann U, Glatzel P, Pushkar Y, Biesiadka J, Loll B, Sauer K, et al. X-ray Damage to the Mn_4Ca Complex in Single Crystals of Photosystem II: A Case Study for Metalloprotein Crystallography. Proc Natl Acad Sci U S A. 2005; 102:12047–12052. [PubMed: 16103362]
29. Mukerji I, Andrews JC, DeRose VJ, Latimer MJ, Yachandra VK, Sauer K, Klein MP. Orientation of the Oxygen-Evolving Manganese Complex in a Photosystem II Membrane Preparation: An X-ray Absorption Spectroscopy Study. Biochemistry. 1994; 33:9712–9721. [PubMed: 8068650]
30. Pushkar Y, Yano J, Glatzel P, Messinger J, Lewis A, Sauer K, Bergmann U, Yachandra V. Structure and Orientation of the Mn_4Ca Cluster in Plant Photosystem II Membranes Studied by Polarized Range-extended X-ray Absorption Spectroscopy. J Biol Chem. 2007; 282:7198–7208. [PubMed: 17190828]
31. Glöckner C, Kern J, Broser M, Zouni A, Yachandra V, Yano J. Structural Changes of the Oxygen-evolving Complex in Photosystem II During the Catalytic Cycle. J Biol Chem. 2013; 288:22607–22620. [PubMed: 23766513]
32. Krewald V, Retegan M, Cox N, Messinger J, Lubitz W, DeBeer S, Neese F, Pantazis DA. Metal Oxidation States in Biological Water Splitting. Chem Sci. 2015; 6:1676–1695.
33. Dismukes GC, Siderer Y. EPR Spectroscopic Observations of a Manganese Center Associated with Water Oxidation in Spinach Chloroplasts. FEBS Lett. 1980; 121:78–80.
34. Casey JL, Sauer K. EPR Detection of a Cryogenically Photogenerated Intermediate in Photosynthetic Oxygen Evolution. Biochim Biophys Acta, Bioenerg. 1984; 767:21–28.
35. Boussac A, Girerd JJ, Rutherford AW. Conversion of the Spin State of the Manganese Complex in Photosystem II Induced by Near-Infrared Light. Biochemistry. 1996; 35:6984–6989. [PubMed: 8679522]
36. Boussac A, Rutherford AW. Comparative Study of the $g = 4.1$ EPR Signals in the S_2 State of Photosystem II. Biochim Biophys Acta, Bioenerg. 2000; 1457:145–156.

37. Haddy A, Lakshmi KV, Brudvig GW, Frank HA. Q-band EPR of the S_2 state of Photosystem II Confirms an $S = 5/2$ Origin of the X-band $g = 4.1$ Signal. Biophys J. 2004; 87:2885–2896. [PubMed: 15454478]
38. Berthold DA, Babcock GT, Yocum CF. A Highly Resolved, Oxygen-evolving Photosystem II Preparation from Spinach Thylakoid Membranes: EPR and Electron-transport Properties. FEBS Lett. 1981; 134:231–234.
39. Ghanotakis DF, Babcock GT, Yocum CF. Calcium Reconstitutes High Rates of Oxygen Evolution in Polypeptide Depleted Photosystem II Preparations. FEBS Lett. 1984; 167:127–130.
40. Ghanotakis DF, Topper JN, Babcock GT, Yocum CF. Water-soluble 17 and 23 kDa Polypeptides Restore Oxygen Evolution Activity by Creating a High-affinity Binding Site for Ca^{2+} on the Oxidizing Side of Photosystem II. FEBS Lett. 1984; 170:169–173.
41. Ono T, Inoue Y. Discrete Extraction of the Ca Atom Functional For O_2 Evolution in Higher Plant Photosystem II by a Simple Low pH Treatment. FEBS Lett. 1988; 227:147–152.
42. Pantazis DA, Orio M, Petrenko T, Zein S, Lubitz W, Messinger J, Neese F. Structure of the Oxygen-evolving Complex of Photosystem II: Information on the S_2 State through Quantum Chemical Calculation of Its Magnetic Properties. Phys Chem Chem Phys. 2009; 11:6788–6798. [PubMed: 19639153]
43. Cox N, Rapatskiy L, Su JH, Pantazis DA, Sugiura M, Kulik L, Dorlet P, Rutherford AW, Neese F, Boussac A, et al. Effect of Ca^{2+}/Sr^{2+} Substitution on the Electronic Structure of the Oxygen-Evolving Complex of Photosystem II: A Combined Multi-frequency EPR, ^{55}Mn-ENDOR, and DFT Study of the S_2 State. J Am Chem Soc. 2011; 133:3635–3648. [PubMed: 21341708]
44. Su JH, Cox N, Ames W, Pantazis DA, Rapatskiy L, Lohmiller T, Kulik LV, Dorlet P, Rutherford AW, Neese F, et al. The Electronic Structures of the S_2 States of the Oxygen-evolving Complexes of Photosystem II in Plants and Cyanobacteria in the Presence and Absence of Methanol. Biochim Biophys Acta, Bioenerg. 2011; 1807:829–840.
45. Lohmiller T, Krewald V, Perez Navarro M, Retegan M, Rapatskiy L, Nowaczyk MM, Boussac A, Neese F, Lubitz W, Pantazis DA, et al. Structure, Ligands and Substrate Coordination of the Oxygen-evolving Complex of Photosystem II in the S_2 State: A Combined EPR and DFT Study. Phys Chem Chem Phys. 2014; 16:11877–11892. [PubMed: 24525937]
46. Hendry G, Wydrzynski T. ^{18}O Isotope Exchange Measurements Reveal that Calcium Is Involved in the Binding of One Substrate-Water Molecule to the Oxygen-Evolving Complex in Photosystem II. Biochemistry. 2003; 42:6209–6217. [PubMed: 12755624]
47. Cox N, Messinger J. Reflections on Substrate Water and Dioxygen Formation. Biochim Biophys Acta, Bioenerg. 2013; 1827:1020–1030.
48. Bovi D, Narzi D, Guidoni L. The S_2 State of the Oxygen-Evolving Complex of Photosystem II Explored by QM/MM Dynamics: Spin Surfaces and Metastable States Suggest a Reaction Path Towards the S_3 State. Angew Chem Int Ed. 2013; 52:11744–11749.
49. Tso J, Sivaraja M, Dismukes GC. Calcium Limits Substrate Accessibility or Reactivity at the Manganese Cluster in Photosynthetic Water Oxidation. Biochemistry. 1991; 30:4734–4739. [PubMed: 1851435]
50. Boussac A, Rutherford AW. S-state Formation after Ca^{2+} Depletion in the Photosystem II Oxygen-evolving Complex. Chem Scr. 1988; 28A:123–126.
51. Vrettos JS, Stone DA, Brudvig GW. Quantifying the Ion Selectivity of the Ca^{2+} Site in Photosystem II: Evidence for Direct Involvement of Ca^{2+} in O_2 Formation. Biochemistry. 2001; 40:7937–7945. [PubMed: 11425322]
52. Rappaport F, Ishida N, Sugiura M, Boussac A. Ca^{2+} Determines the Entropy Changes Associated with the Formation of Transition States during Water Oxidation by Photosystem II. Energy Environ Sci. 2011; 4:2520–2524.
53. Retegan M, Cox N, Lubitz W, Neese F, Pantazis DA. The First Tyrosyl Radical Intermediate Formed in the S_2-S_3 Transition of Photosystem II. Phys Chem Chem Phys. 2014; 16:11901–11910. [PubMed: 24760184]
54. Kuwabara T, Murata N. Inactivation of Photosynthetic Oxygen Evolution and Concomitant Release of Three Polypeptides in the Photosystem II Particles of Spinach Chloroplasts. Plant Cell Physiol. 1982; 23:533–539.

55. Rutherford AW. Orientation of EPR Signals Arising from Components in Photosystem II Membranes. Biochim Biophys Acta, Bioenerg. 1985; 807:189–201.
56. Andrews, JC. PhD Thesis. University of California; Berkeley, CA: 1995. X-ray Absorption Spectroscopy and EPR Studies of Oriented Spinach Thylakoid Preparations.
57. Goodin, DB.; Falk, KE.; Wydrzynski, T.; Klein, MP. 6th Annual Stanford Synchrotron Radiation Laboratory Users Group Meeting. Vol. 79/05. Stanford University; Stanford, CA: 1979. p. 10-11.
58. Webb SM. SIXpack: A Graphical User Interface for XAS Analysis Using IFEFFIT. Phys Scr. 2005; T115:1011–1014.
59. Rehr JJ, Albers RC. Theoretical Approaches to X-ray Absorption Fine Structure. Rev Mod Phys. 2000; 72:621–654.
60. Rutherford AW, Zimmermann JLA. New EPR Signal Attributed to the Primary Plastosemiquinone Acceptor in Photosystem II. Biochim Biophys Acta, Bioenerg. 1984; 767:168–175.
61. Schiller H, Dittmer J, Iuzzolino L, Dörner W, Meyer-Klaucke W, Solé VA, Nolting HF, Dau H. Structure and Orientation of the Oxygen-Evolving Manganese Complex of Green Algae and Higher Plants Investigated by X-ray Absorption Linear Dichroism Spectroscopy on Oriented Photosystem II Membrane Particles. Biochemistry. 1998; 37:7340–7350. [PubMed: 9585548]
62. Goodin DB, Yachandra VK, Britt RD, Sauer K, Klein MP. The State of Manganese in the Photosynthetic Apparatus. 3. Light-induced Changes in X-ray Absorption (K-Edge) Energies of Manganese in Photosynthetic Membranes. Biochim Biophys Acta, Bioenerg. 1984; 767:209–216.
63. Yachandra VK, Guiles RD, Mcdermott A, Britt RD, Dexheimer SL, Sauer K, Klein MP. The State of Manganese in the Photosynthetic Apparatus: 4. Structure of the Manganese Complex in Photosystem II Studied Using EXAFS Spectroscopy. The S_1 State of the O_2-Evolving Photosystem II Complex from Spinach. Biochim Biophys Acta, Bioenerg. 1986; 850:324–332.
64. Yachandra VK, Guiles RD, Mcdermott AE, Cole JL, Britt RD, Dexheimer SL, Sauer K, Klein MP. Comparison of the Structure of the Manganese Complex in the S_1 and S_2 States of the Photosynthetic O_2-Evolving Complex: An X-ray Absorption Spectroscopy Study. Biochemistry. 1987; 26:5974–5981. [PubMed: 3318924]
65. Guiles RD, Yachandra VK, Mcdermott AE, Cole JL, Dexheimer SL, Britt RD, Sauer K, Klein MP. The S_0 State of Photosystem II Induced by Hydroxylamine: Differences between the Structure of the Manganese Complex in the S_0 and S_1 States Determined by X-ray Absorption Spectroscopy. Biochemistry. 1990; 29:486–496. [PubMed: 2154248]
66. Pennerhahn JE, Fronko RM, Pecoraro VL, Yocum CF, Betts SD, Bowlby NR. Structural Characterization of the Manganese Sites in the Photosynthetic Oxygen-Evolving Complex Using X-ray Absorption Spectroscopy. J Am Chem Soc. 1990; 112:2549–2557.
67. Maclachlan DJ, Hallahan BJ, Ruffle SV, Nugent JHA, Evans MCW, Strange RW, Hasnain SS. An e.x.a.f.s. Study of the Manganese O_2-Evolving Complex in Purified Photosystem II Membrane Fractions - the S_1 and S_2 States. Biochem J. 1992; 285:569–576. [PubMed: 1637347]
68. Maclachlan DJ, Nugent JHA, Evans MCW. A XANES Study of the Manganese Complex of Inhibited PS II Membranes Indicates Manganese Redox Changes between the Modified S_1, S_2 and S_3 States. Biochim Biophys Acta, Bioenerg. 1994; 1185:103–111.
69. Iuzzolino L, Dittmer J, Dorner W, Meyer-Klaucke W, Dau H. X-ray Absorption Spectroscopy on Layered Photosystem II Membrane Particles Suggests Manganese-Centered Oxidation of the Oxygen-Evolving Complex for the S_0-S_1, S_1-S_2, and S_2-S_3 Transitions of the Water Oxidation Cycle. Biochemistry. 1998; 37:17112–17119. [PubMed: 9860823]
70. Ono T, Kusunoki M, Matsushita T, Oyanagi H, Inoue Y. Structural and Functional Modifications of the Manganese Cluster in Ca^{2+}-Depleted S_1 and S_2 States: Electron Paramagnetic Resonance and X-ray Absorption Spectroscopy Studies. Biochemistry. 1991; 30:6836–6841. [PubMed: 1648962]
71. Ono TA, Noguchi T, Inoue Y, Kusunoki M, Yamaguchi H, Oyanagi H. Flash Induced XANES Spectroscopy for the Ca-depleted Mn-cluster in the Photosynthetic O_2-evolving Enzyme. FEBS Lett. 1993; 330:28–30. [PubMed: 8396538]
72. Maclachlan DJ, Nugent JHA, Bratt PJ, Evans MCW. The Effects of Calcium Depletion on the O_2-Evolving Complex in Spinach PS II: the S_1*, S_2* and S_3* States and the Role of the 17 kDa and 23 kDa Extrinsic Polypeptides. Biochim Biophys Acta, Bioenerg. 1994; 1186:186–200.

73. Kanady JS, Tsui EY, Day MW, Agapie T. A Synthetic Model of the Mn_3Ca Subsite of the Oxygen-Evolving Complex in Photosystem II. Science. 2011; 333:733–736. [PubMed: 21817047]
74. Saito K, Ishikita H. Influence of the Ca^{2+} Ion on the Mn_4Ca Conformation and the H-bond Network Arrangement in Photosystem II. Biochim Biophys Acta. 2014; 1837:159–166. [PubMed: 24095684]
75. Siegbahn PEM. Water Oxidation Energy Diagrams for Photosystem II for Different Protonation States, and the Effect of Removing Calcium. Phys Chem Chem Phys. 2014; 16:11893–11900. [PubMed: 24618784]
76. Yang J, Hatakeyama M, Ogata K, Nakamura S, Li C. Theoretical Study on the Role of Ca^{2+} at the S_2 State in Photosystem II. J Phys Chem B. 2014; 118:14215–14222. [PubMed: 25357007]
77. Yano J, Pushkar Y, Glatzel P, Lewis A, Sauer K, Messinger J, Bergmann U, Yachandra V. High-Resolution Mn EXAFS of the Oxygen-Evolving Complex in Photosystem II: Structural Implications for the Mn_4Ca Cluster. J Am Chem Soc. 2005; 127:14974–14975. [PubMed: 16248606]
78. Dekker JP, Ghanotakis DF, Plijter JJ, Vangorkom HJ, Babcock GT. Kinetics of the Oxygen-evolving Complex in Salt-washed Photosystem II Preparations. Biochim Biophys Acta, Bioenerg. 1984; 767:515–523.
79. Narzi D, Bovi D, Guidoni L. Pathway for Mn-cluster Oxidation by Tyrosine-Z in the S_2 state of Photosystem II. Proc Natl Acad Sci U S A. 2014; 111:8723–8728. [PubMed: 24889635]
80. Cox N, Retegan M, Neese F, Pantazis DA, Boussac A, Lubitz W. Electronic Structure of the Oxygen-evolving Complex in Photosystem II prior to O-O Bond Formation. Science. 2014; 345:804–808. [PubMed: 25124437]
81. Siegbahn PEM. Water Oxidation Mechanism in Photosystem II, Including Oxidations, Proton Release Pathways, O-O Bond Formation and O_2 Release. Biochim Biophys Acta, Bioenerg. 2013; 1827:1003–1019.
82. Pérez Navarro M, Ames WM, Nilsson H, Lohmiller T, Pantazis DA, Rapatskiy L, Nowaczyk MM, Neese F, Boussac A, Messinger J, et al. Ammonia Binding to the Oxygen-evolving Complex of Photosystem II Identifies the Solvent-Exchangeable Oxygen Bridge (μ-oxo) of the Manganese Tetramer. Proc Natl Acad Sci U S A. 2013; 110:15561–15566. [PubMed: 24023065]
83. Miqyass M, van Gorkom HJ, Yocum CF. The PSII Calcium Site Revisited. Photosynth Res. 2007; 92:275–287. [PubMed: 17235491]
84. Rapatskiy L, Cox N, Savitsky A, Ames WM, Sander J, Nowaczyk MM, Rogner M, Boussac A, Neese F, Messinger J, et al. Detection of the Water-Binding Sites of the Oxygen-Evolving Complex of Photosystem II Using W-Band ^{17}O Electron-Electron Double Resonance-Detected NMR Spectroscopy. J Am Chem Soc. 2012; 134:16619–16634. [PubMed: 22937979]
85. Siegbahn PEM. Structures and Energetics for O_2 Formation in Photosystem II. Acc Chem Res. 2009; 42:1871–1880. [PubMed: 19856959]

Abbreviations

CW	continuous wave
EPR	electron paramagnetic resonance
EXAFS	extended X-ray absorption fine structure
IPE	inflection point energy
MLS	multiline EPR signal
OEC	oxygen-evolving complex
PS II	photosystem II
XANES	X-ray absorption near-edge structure

XAS	X-ray absorption spectroscopy
XFEL	X-ray free-electron laser
XRD	X-ray diffraction

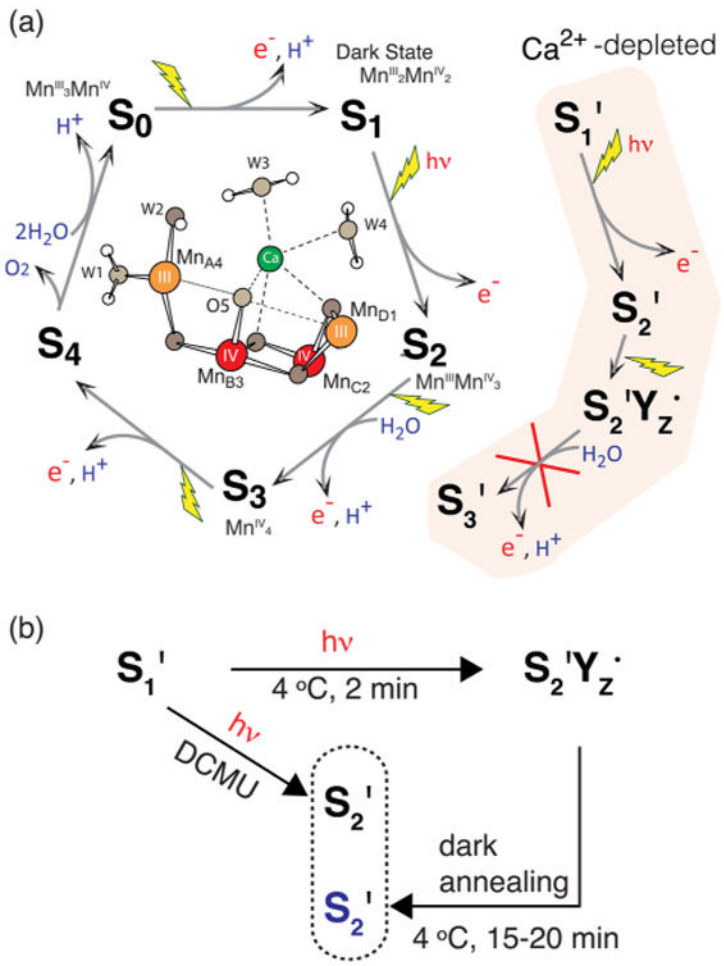

Figure 1.

(A) The S-state cycle in native PS II and the S′-state cycle of Ca^{2+}-depleted PS II, inhibited after the $S_2'Y_Z^{\bullet}$ state, as well as a schematic view of the OEC in the S_1 state. (B) S′-state advancement in Ca^{2+}-depleted PS II samples including two different methods to generate the S_2' state, by dark-adaptation and in the presence of 3-(3,4-dichlorophenyl)-1,1-dimethylurea (DCMU), a herbicide that blocks electron transfer from acceptor quinone Q_A to Q_B, thus allowing advancement of the OEC only to S_2 in native PS II or S_2' in Ca^{2+}-depleted PS II.

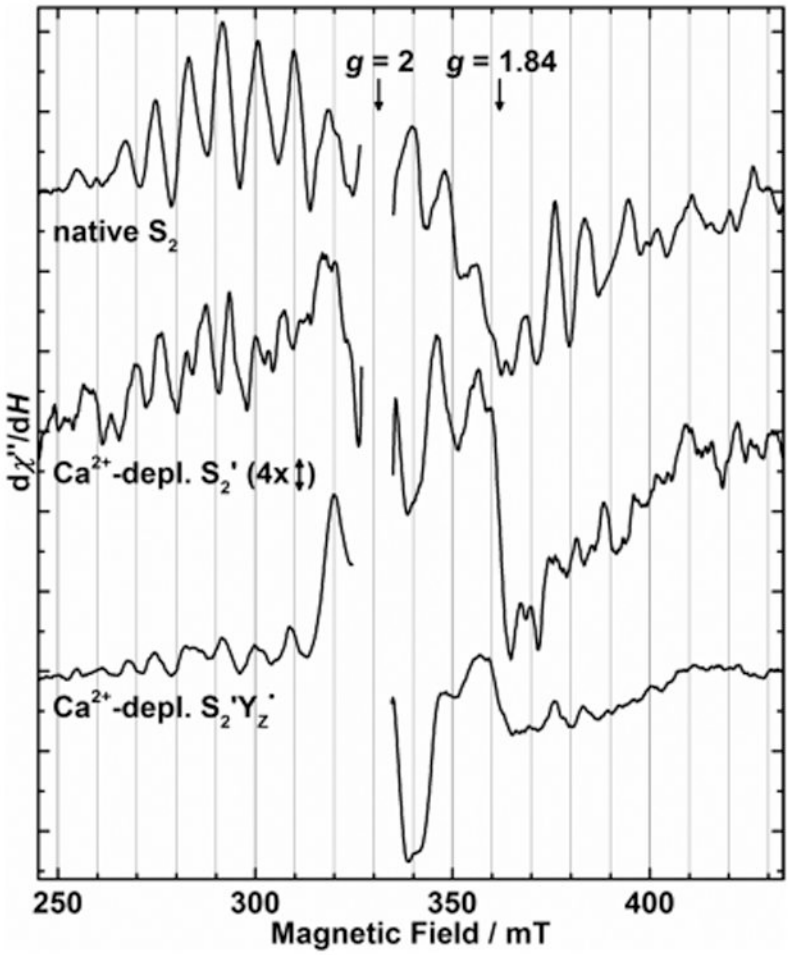

Figure 2.

EPR light-minus-dark difference spectra of the native S_2 state and Ca^{2+}-depleted samples in the S_2' and $S_2'Y_Z^{\bullet}$ states (top to bottom). Due to its inherently smaller signal amplitude, the S_2' altered MLS is displayed on a four times expanded vertical scale. The overlapping $Y_D^{\bullet}$ signal ($g = 2$) was excised for clarity of presentation. At $g \approx 1.84$, contributions from the Q_A^{-}-Fe^{2+} semiquinone-iron cofactor[60] were present in all samples. Continuous illumination conditions are as follows. S_2 (top): 195 K, 20 min; S_2' (middle): 4 °C, 2 min + 15 min dark-adaptation; and $S_2'Y_z^{\bullet}$ (bottom): 4 °C, 2 min. EPR conditions: microwave frequency, 9.28 GHz; microwave power, 30 mW; modulation amplitude, 32 G; and temperature, 8 K.

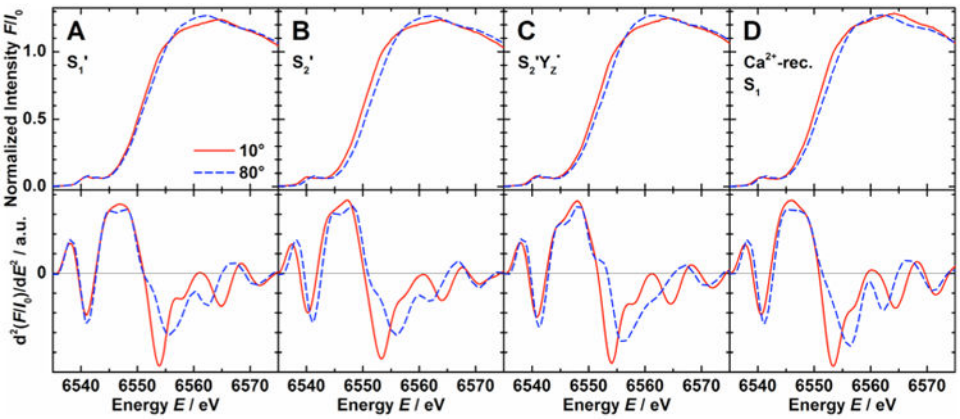

Figure 3.

Mn K-edge absorption spectra (top) and corresponding second derivatives (bottom) of one-dimensionally ordered Ca^{2+}-depleted (A) S_1', (B) S_2', and (C) $S_2'Y_Z^{\bullet}$, and (D) Ca^{2+}-reconstituted S_1 state samples at orientations θ of 10° (solid red lines) and 80° (dashed blue lines).

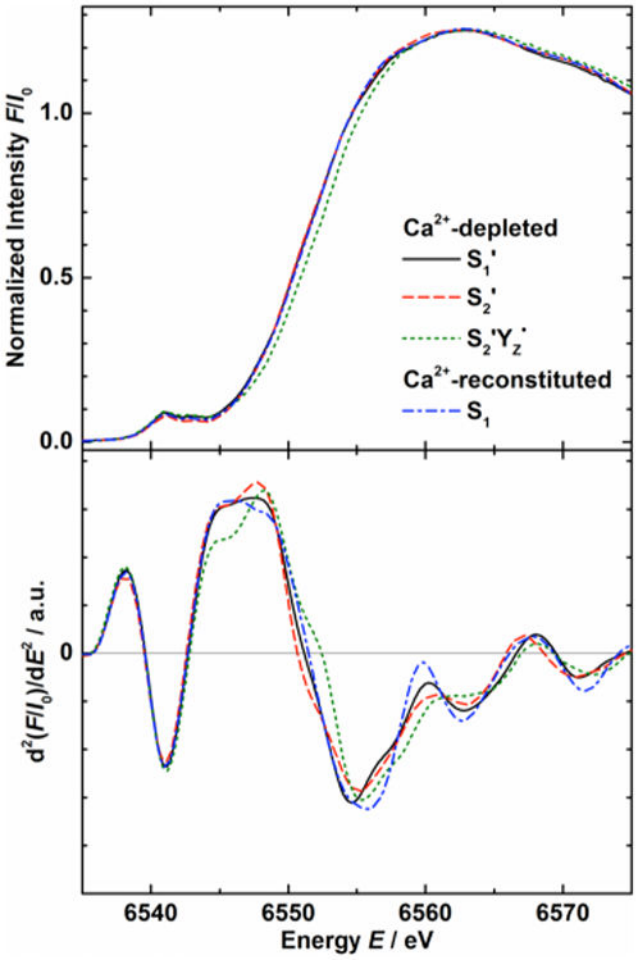

Figure 4.

Isotropic Mn K-edge absorption spectra and corresponding second derivatives from Ca^{2+}-depleted S_1' (solid black lines), S_2' (dashed red lines), and $S_2'Y_Z^{\bullet}$ (dotted green lines), and Ca^{2+}-reconstituted S_1 state samples (dash-dotted blue lines). The spectra were calculated based on polarized data (10° and 80°, Figure 3) and isotropic spectra from nonoriented PS II samples (54.7°, Figure S3 of the Supporting Information).

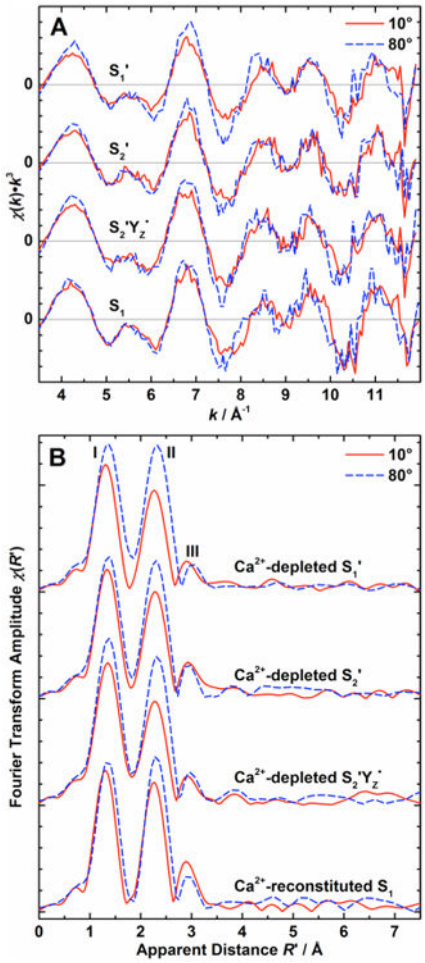

Figure 5.

(A) k^3-weighted EXAFS spectra and (B) Fourier transforms of the k^3-weighted EXAFS spectra of one-dimensionally ordered Ca^{2+}-depleted states S_1', S_2', $S_2'Y_Z^{\bullet}$, and Ca^{2+}-reconstituted S_1 state samples (top to bottom) at $\theta = 10°$ (solid red lines) and 80° (dashed blue lines). For Fourier transformation to R'-space, the k-space limits were set to the zero crossings of the lowest (~3.6 $Å^{-1}$) and highest (11.2–11.9 $Å^{-1}$) k in this region.

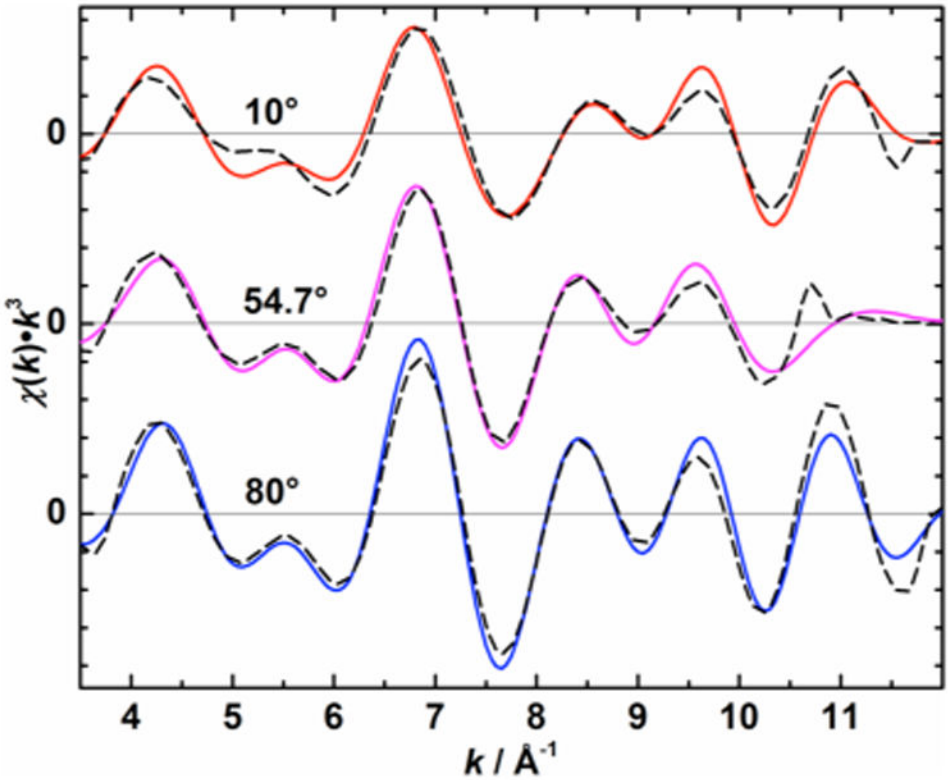

Figure 6.

Fourier isolates (0.9 Å < R' < 3.5 Å, solid colored lines) and corresponding EXAFS curve fitting results (dashed black lines) of a one-dimensionally ordered S_1' state sample at $\theta = 10°$ (top) and 80° (bottom), and a nonordered S_1' sample ($\theta = 54.7°$, middle).

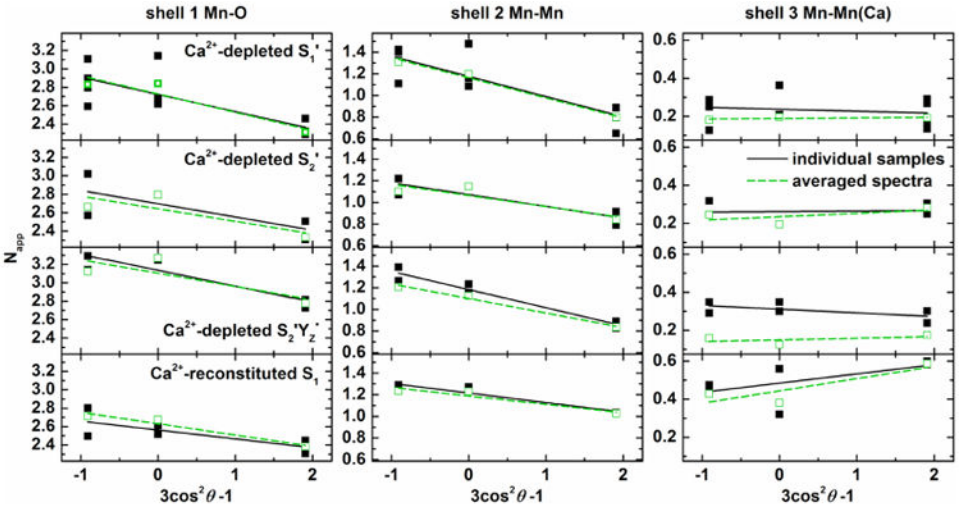

Figure 7.

Linear plots of the apparent coordination numbers N_{app} vs $3\cos^2\theta - 1$ and corresponding fit curves for shells j = 1–3 of Ca^{2+}-depleted S_1', S_2', $S_2'Y_Z^{\bullet}$, and Ca^{2+}-reconstituted S_1 state samples (top to bottom) both from spectra of individual samples (black) and from averages thereof (green). θ = 10° and 80° correspond to x = 1.9 and −0.9, respectively, in this representation. The magic angle $\theta \approx 54.7°$ corresponds to x = 0, so that the intercept of the y axis equals N_{iso}.

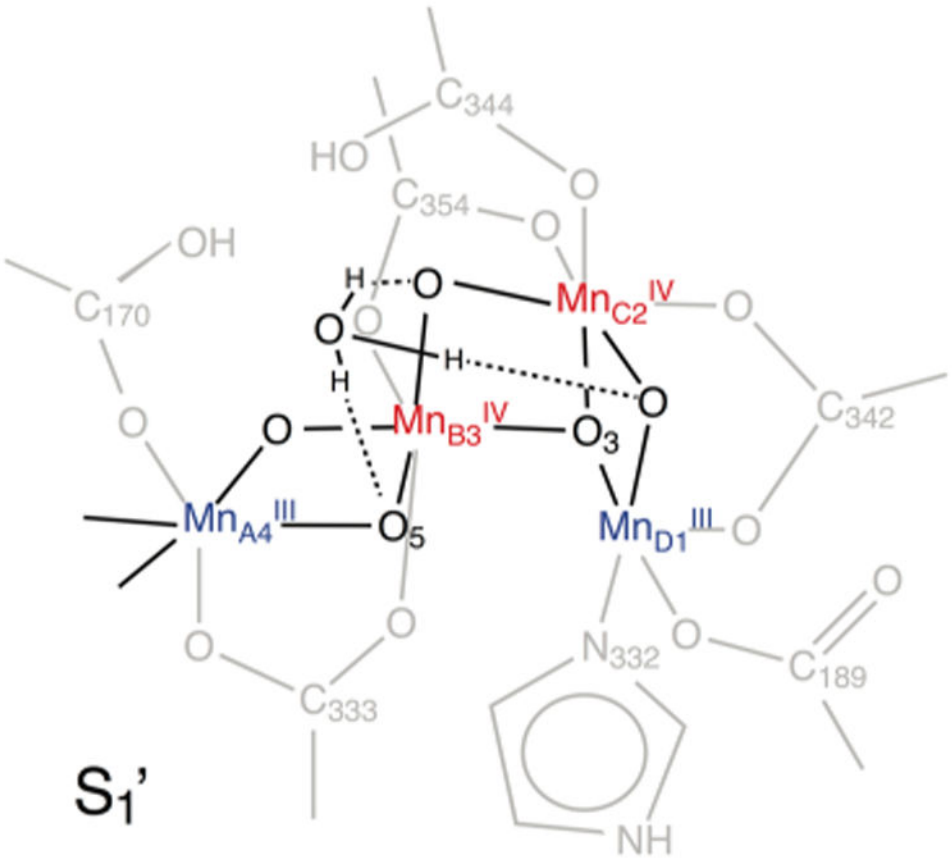

Figure 8.

Structural model of the Ca^{2+}-depleted OEC in the S_1' state with a possible H_3O^+ ion in place of the Ca^{2+} ion present in the native OEC.

Table 1

IPE Values in eV of Anisotropic Samples at Orientations θ of 10° and 80° and Isotropic Values (from Isotropic Samples, Corresponding to an Angle of 54.7°, as well as Calculated by Linear Regression Analysis of the Experimental Values[a])[b]

		10°	80°	54.7°	isotropic
Ca^{2+}-depleted	S_1'	6551.2 ± 0.6 (4)	6551.8 ± 1.1 (4)	6551.3 ± 0.1 (3)	6551.5 ± 0.2
	S_2'	6550.3 ± 0.4 (2)	6551.1 ± 0.6 (2)	6550.8 (1)	6550.8 ± 0.2
	$S_2'Y_Z^{\bullet}$	6551.6 ± 0.1 (2)	6553.3 ± 0.0 (2)	6552.4 ± 0.6 (2)	6552.6 ± 0.1
Ca^{2+}-reconstituted	S_1	6550.8 ± 0.4 (2)	6551.7 ± 0.9 (2)	6551.8 ± 0.0 (2)	6551.6 ± 0.2

[a] These averages of the IPE values of the individual samples differ insignificantly from the energies of the zero crossings of the corresponding averaged second derivative curves (Figures 3 and 4 and Figure S3 of the Supporting Information) due to the not completely identical averaging methods.

[b] Numbers of samples given in parentheses.

Table 2

Polarized EXAFS Fit Parameters R_j and $N_{app,j}$ of the Coordination Shells j = 1–3 from Fits to Spectra of Individual Samples at the Different Orientations θ[a,b]

state	θ	shell 1 Mn–O		shell 2 Mn–Mn		shell 3 Mn–Mn(Ca)	
		R_1 (Å)	$N_{app,1}$	R_2 (Å)	$N_{app,2}$	R_3 (Å)	$N_{app,3}$
S_1'	10°	1.84(1)	2.3(1)	2.70(1)	0.8(1)	3.27(4)	0.2(1)
	54.7°	1.85(2)	2.8(3)	2.72(2)	1.2(2)	3.24(4)	0.3(1)
	80°	1.87(1)	2.8(2)	2.75(1)	1.3(1)	3.31(5)	0.2(1)
S_2'	10°	1.85(1)	2.4(1)	2.71(0)	0.9(1)	3.29(2)	0.3(0)
	54.7°	1.85	2.8	2.72	1.1	3.27	0.2
	80°	1.86(0)	2.8(3)	2.73(0)	1.1(1)	3.27(0)	0.3(1)
$S_2'Y_Z^{\bullet}$	10°	1.87(0)	2.8(1)	2.73(0)	0.9(0)	3.29(1)	0.3(0)
	54.7°	1.87(2)	3.2(0)	2.74(3)	1.2(1)	3.30(2)	0.3(0)
	80°	1.88(1)	3.2(1)	2.76(1)	1.3(1)	3.32(3)	0.3(0)
S_1	10°	1.83(0)	2.4(1)	2.70(0)	1.0(0)	3.27(1)	0.6(0)
	54.7°	1.85(0)	2.6(1)	2.73(1)	1.3(0)	3.25(0)	0.4(2)
	80°	1.86(1)	2.6(2)	2.74(0)	1.3(0)	3.25(1)	0.5(0)

[a] Standard deviations are reported in parentheses as the uncertainty in the least significant digit, except for the parameters from the single nonordered S_2' state sample.

[b] The Debye–Waller factors σ_j used for all samples were 0.006 $Å^2$ for the Mn–O/N interactions of peak I, 0.003 $Å^2$ for the Mn–Mn interactions of peak II, as well as for the Mn–Mn interaction of peak III in Ca^{2+}-depleted samples, and 0.004 $Å^2$ for the Mn–Mn(Ca) interactions of peak III in Ca^{2+}-reconstituted samples owing to the increased number of ligand atoms in the same shell.

Table 3

$N_{iso,j}$ and φ_j for the Various Sample States from Linear Regression Analysis, as well as R_j Averaged over All Samples in a Particular State[a]

state	shell 1 Mn–O			shell 2 Mn–Mn			Shell 3 Mn–Mn(Ca)		
	R_1 (Å)	$N_{iso,1}$	φ_1 (°)	R_2 (Å)	$N_{iso,2}$	φ_2 (°)	R_3 (Å)	$N_{iso,3}$	φ_3 (°)
S_1'	1.85(2)	2.7(1)	58	2.72(2)	1.2(0)	64	3.28(5)	0.2(0)	57
S_2'	1.86(1)	2.7(1)	58	2.72(1)	1.1(0)	60	3.28(2)	0.3(0)	54
$S_2'Y_Z^{\bullet}$	1.87(1)	3.1(0)	58	2.74(2)	1.2(0)	63	3.30(2)	0.3(0)	58
S_1	1.85(1)	2.6(1)	57	2.72(2)	1.2(0)	59	3.26(1)	0.5(0)	50
native S_1[b]				2.74(2)	1.3(3)	63(5)	3.20(2)[b]	0.4(1)[b]	>70[b]

[a] Standard deviations are given in parentheses.

[b] Parameters for the native S_1 state Mn_4O_5Ca cluster from ref 30. The numbers given for shell 3 represent the Mn-μO-Mn contribution only, extracted by range-extended Mn K-edge EXAFS.